

Main sequence of star formation and colour bimodality considering galaxy environment

Pius Privatus^{1,2,*} and Umananda Dev Goswami^{1,†}

¹*Department of Physics, Dibrugarh University, Dibrugarh 786004, Assam, India*

²*Department of Natural Sciences, Mbeya University of Science and Technology, Iyunga, 53119, Mbeya, Tanzania*

This study involves the use of Sloan Digital Sky Survey Data Release 12 (SDSS DR12) also referred to as the Legacy Survey to investigate the influence of the galaxy environment on the main sequence of star formation, colour bimodality and the quenching of star formation rate. We classify the galaxies according to the ratio of their emission lines and based on their environment (isolated and non-isolated). We find that for $z \lesssim 0.09$, the fraction of non-isolated galaxies is greater than isolated galaxies, whereas for $z > 0.09$ the opposite result is observed. Quenching is observed to be influenced by the environment at $M_* < 10^{10.7} M_\odot$ (mostly for the star-forming and composite galaxies), while for $M_* \geq 10^{10.7} M_\odot$ (mostly for Seyfert galaxies and low-ionization nuclear emission-line regions), the effect of the environment is very weak. We observe the decrease in the slope of the star formation main sequence by ~ 0.02 dex and the intercept by ~ 0.17 dex for non-isolated galaxies in comparison to isolated galaxies. We also find that star-forming, composite, Seyfert galaxies and low-ionization nuclear emission-line regions form the evolutionary pathways, where most star-forming galaxies ($\sim 60\%$) are found in the blue cloud, both composite ($\sim 50\%$) and Seyfert ($\sim 49\%$) galaxies in the green valley and low-ionization nuclear emission-line regions ($\sim 60\%$) in the red sequence. The study concludes that the environment in which the galaxies reside influences the shape of the star formation main sequence, quenching and hence colour bimodality especially for star-forming and composite galaxies while for Seyfert and low-ionization nuclear emission-line region galaxies, there is a mild impact.

Keywords: Main sequence; Colour bimodality; Green valley; Galaxy environment.

I. INTRODUCTION

The star-forming (SF) main sequence (MS) refers to a close relationship between the rates at which stars are formed and the changes in the masses of stars (M_* s) in the majority of the galaxy population undergoing star formation. The baseline of the correlation between these two parameters changes over time, indicating that the intensity of star formation changes significantly with time. There is considerable uncertainty regarding the slope and dispersion of this correlation. The literature presents different values of slope between 0.2 and 1.2, and the dispersion, ranging from 0.3 to 0.6 [1]. The predominant source of uncertainty arises from the biases introduced through various factors. These may include the criteria employed for selecting the SF galaxy population, the indicators used for the star formation rates (SFRs), the fitting method applied (such as mean, median, or mode), and the non-linearity of the relation, where the slope varies across different mass scales.

A comprehensive understanding of how the MS evolves is crucial for capturing fundamental insights into how galaxies grow. In this regard, the slope of the correlation between SFR and M_* provides information on how star formation activity changes across diverse stellar masses, while the dispersion of this correlation unveils the degree of unpredictability in the history of gas accretion and the efficiency of star formation [2–7]. Therefore, comprehending the trajectory of galaxies over time in the SFR versus M_* plane serves as a potential tool for identifying the processes responsible for the gradual decline in star formation activity as time progresses.

The fitting parameters of the MS provide information about the nature of stellar mass buildup and star formation where the slope is related to the slope of low mass SF galaxies and the normalization of the MS evolution is thought to be due to the evolution of gas density with redshift [1, 8–10]. Refs. [11, 12] revealed that the MS requires a more complex stellar mass fit. By selecting the SF galaxies from the seventh release of SDSS data with the range of redshift $0.02 < z < 0.085$ Ref. [13] obtained the absence of deviation from the simple power-law MS relation in the local galaxies. This study revealed that the deviation originates from the inconsistency in SF galaxies' selection, however in this study the active galactic nucleus (AGN) galaxies were excluded from the analysis and only the SF galaxies were discussed.

Moreover, the galaxy colour versus stellar mass which serves as a potential tool for identifying the mechanism deriving this bimodality [14], is another very important subject to undertake. Different studies tried to include the AGNs in the colour versus stellar mass diagram and obtained that these galaxies populate the red sequence and the state between blue cloud and red sequence which is known as green valley. For example, Ref. [15] obtained that the inclusion of AGNs in these diagrams enable to obtain the role of AGN's feedback in the quenching of SFR of early type galaxies. Ref. [16] obtained that the AGNs are populated on a distinct region of the colour versus stellar mass diagram referred to as the red sequence or top of the blue cloud,

* Email: privatuspius08@gmail.com

† Email: umananda2@gmail.com

believing that a key stage in the massive galaxies’ evolution is the quenching of SFR at which there is the migration of blue cloud to the red sequence. Ref. [16] outlined that AGNs may be the cause or they maintain the quenching process. Furthermore, the ongoing star formation is not a necessary condition for the AGN activity since the black holes’ accretions are observed when the star formation has been terminated.

In a simplified representation, the process guiding these transformation can be broadly categorized as ‘internal’ and ‘external’. The ongoing debate revolves around the extent to which each of these scenarios influences galaxy properties. The internal process involves the co-evolution of a galaxy and its black hole. The majority of galaxy formation models observe AGN feedback to be a primary mechanism affecting the main sequence [17]. Although this mechanism may have an impact in the case of massive galaxies exceeding 10^{11} solar masses, there is a lack of observed feedback effects for the majority of the SF galaxies [18]. On the other hand, external processes involve processes associated with interactions either among more than one galaxy or with the surrounding environment. Both internal and external processes have undergone extensive studies in the literature [19–28].

Ref. [26] observed morphology quenching to be a reason for the reduction of star formation activities in galaxies mainly as a bulge formation which stabilizes the gas disc against the gravitational instabilities. Ref. [27] obtained that morphology and environment have a combined role in slowing down the star formation activities in galaxies. Furthermore, they observed that a long-time scale environmental effect appears at low redshift. Ref. [28] suggested that the quenching of SFR is mainly due to internal and linked with bulge growth. However, the existence of the relation between morphology and density may provide a different turn in the relation of SFR, stellar mass and the environment where a particular galaxy resides. These studies aim to discern the mechanism or combination of mechanisms that lead to the quenching of star formation processes in galaxies, thereby influencing their evolution. Despite the fact that to build a global picture of the galaxy evolution involves understanding of how the evolution of galaxy and environment are related. Currently, there is still a deficiency of comprehensive studies relating the positioning of galaxies with respect to the MS for different environments.

In this paper, our primary goal is to investigate whether the positioning of galaxies on the star formation MS depends on the galaxy environment by using isolated and non-isolated galaxy samples. Additionally, we aim to quantify the evolutionary trajectory of composite, Seyfert (Seyfert 1 not included), and low-ionization nuclear emission-line region (LINER) galaxies with respect to the colour-stellar mass diagram, seeking insights into whether galaxy environment plays a role in shaping galaxy colour bimodality. The width of the MS is defined as ± 0.3 dex ranging from the best fit line of SFR– M_* plane. This approach enables us to assess the linearity of the MS and explore the dispersion of the MS.

The structure of this paper is as follows: In the next section, we explain the source of data and the method of getting samples. Section III is dedicated to presenting the results. In Section IV the results are discussed. Section V presents the summary and conclusion. Cosmological constants are adopted from Ref. [29], wherein the dark energy density parameter $\Omega_\Lambda = 0.692$, Hubble constant of $H_0 = 67.8 \text{ km s}^{-1} \text{ Mpc}^{-1}$ and the matter density parameter $\Omega_m = 0.308$ are recorded.

II. DATA AND ANALYSIS

In this research work the catalog data extracted from the twelfth release of Sloan Digital Sky Survey (SDSS DR12) as detailed in Refs. [30, 31] specifically, the value added catalog detailed in Refs. [32, 33] was employed. This catalog contains 584 449 galaxies which are either in groups, clusters or isolated up to $z = 0.2$, all brighter than Petrosian r-band magnitude of 17.77. We performed 1 arcsec cross-correlation between the data obtained from the methods outlined in Ref. [32] and the Max Planck Institute for Astrophysics and Johns Hopkins University (MPA-JHU) to obtain a total of 571 459 galaxies that satisfy the requisite cut-off condition. We applied a signal-to-noise condition of 3 for [OIII] λ 5007, [NII] λ 6584 spectral lines, and the Balmer recombination lines including $H\alpha$ and $H\beta$ resulting in a total of 274 517 galaxies.

The stellar masses obtained from the MPA-JHU team were calculated from the Bayesian approach as detailed in Ref. [34]. Stellar mass calculation within the SDSS spectroscopic fiber aperture relies on the fiber magnitudes, whereas the total stellar mass is determined using the model magnitudes. The MPA-JHU total SFR used in this study was derived from the MPA-JHU database and estimated using the methods of Refs. [35, 36] with adjustments made for non SF galaxies. The MPA-JHU team uses the $H\alpha$ calibration [37] to determine the SFR for galaxies classed as SF. In contrast to the approach taken by Ref. [35], the MPA-JHU team applied aperture corrections for SFR by fitting the photometric data from the outer regions of the galaxies. Specifically, for SFR computation, Ref. [35] outlined the calculation within the galaxy fiber aperture. It is important to keep in mind that the region beyond the fiber SFR is estimated using the methods of Ref. [38]. Furthermore, for the case of AGN and weak emission line galaxies, SFR was determined using photometry. Although the output for stellar mass and SFR are presented in probability distribution functions at 2.5%, 16%, 50%, 84%, and 97.5% values, in this study we use the median estimates (50%) of the probability distributions. The galaxies having no M_* and SFR and the specific star formation rate (SSFR) measurements were removed from the sample making a total of 268 954 galaxies. We classify the galaxies using the *NII* diagnostic diagram as

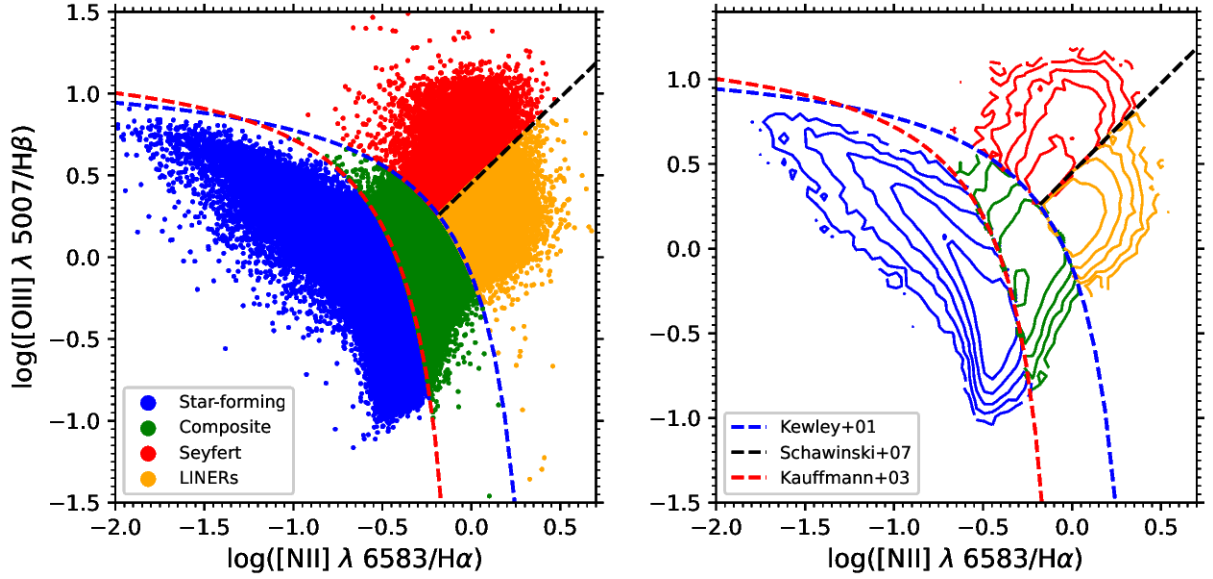


FIG. 1. The diagnostic diagram for all the classified galaxies with the scatter plot (left panel) and the contour plot (right panel).

detailed in Ref. [15, 39–41], which is based on the following equations:

$$\log_{10} \left(\frac{[\text{OIII}]}{H\beta} \right) < 0.61 \left(\log_{10} \left(\frac{[\text{NII}]}{H\alpha} \right) - 0.05 \right)^{-1} + 1.3, \quad (1)$$

$$\log_{10} \left(\frac{[\text{OIII}]}{H\beta} \right) < 0.61 \left(\log_{10} \left(\frac{[\text{NII}]}{H\alpha} \right) - 0.47 \right)^{-1} + 1.19, \quad (2)$$

$$\log_{10} \left(\frac{[\text{OIII}]}{H\beta} \right) > 0.61 \left(\log_{10} \left(\frac{[\text{NII}]}{H\alpha} \right) - 0.47 \right)^{-1} + 1.19, \quad (3)$$

$$\log_{10} \left(\frac{[\text{OIII}]}{H\beta} \right) - 0.45 < 1.05 \left(\log_{10} \left(\frac{[\text{NII}]}{H\alpha} \right) \right). \quad (4)$$

Here, SF galaxies were obtained by Eq. (1), composite galaxies by Eq. (2), AGN galaxies by Eq. (3), while the Seyfert and LINER galaxies were discerned from AGNs by using Eq. (4). After application of all stated procedures, the sample contains 170 797 (63%) SF, 58 763 (22%) composite, 12 536 (5%) Seyfert and 26 858 (10%) LINERs. The distribution of galaxies is shown in the diagnostic diagram in Fig. 1.

The galaxies with no neighbour (with $N_{gal} = 1$ flag) are isolated, while the galaxies with more than one neighbour (with $N_{gal} \geq 2$ flag) are non-isolated. The final dataset contains 93 727 (55%) isolated, 77 070 (45%) non-isolated SF galaxies; 30 652 (52%) isolated, 28 111 (48%) non-isolated composite galaxies; 6 643 (53%) isolated, 5 893 (47%) non-isolated Seyfert galaxies; and 11 355 (42%) isolated, 15 503 (58%) non-isolated LINER galaxies. The distribution of galaxies according to redshift in the final sample for isolated galaxies and non-isolated galaxies is shown in Fig. 2. From this figure, it is observed that the number of non-isolated galaxies in the lower redshift range ($z < 0.09$) is larger than the isolated, while in the higher redshift range ($z \geq 0.09$) the number of isolated galaxies is higher than the number of non-isolated galaxies. This indicates that isolated galaxies are preferentially found at higher redshift while non-isolated galaxies are found at lower redshift.

III. RESULTS

A. The Main Sequence (MS)

The relationship between the SFR and stellar mass M_* serves as the tracer on how the stars are formed in relation to the stellar mass within a galaxy. The MS is generally characterized by such a relation as given by

$$\log_{10}(\text{SFR}) = \beta \log_{10}(M_*) + \alpha, \quad (5)$$

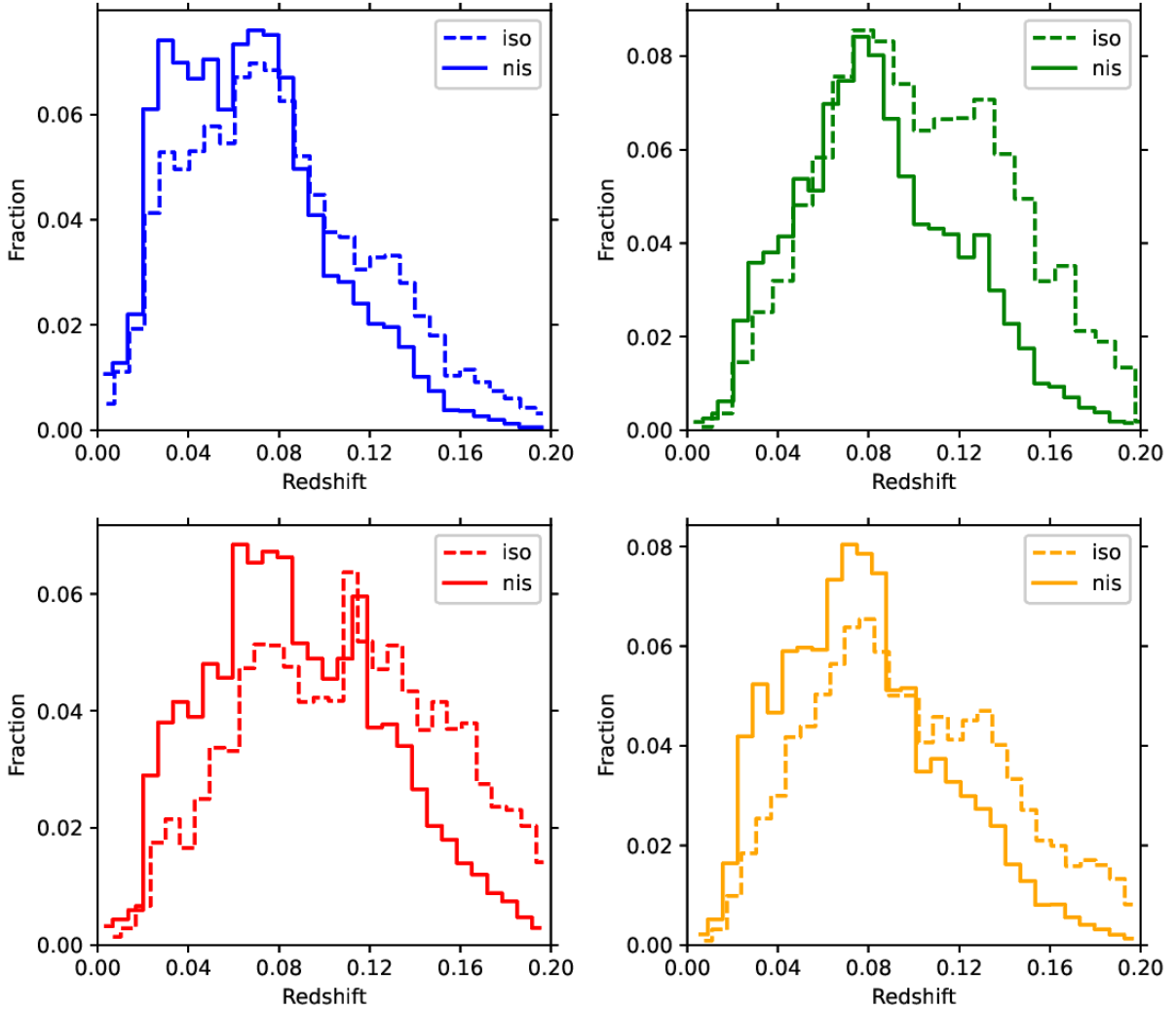


FIG. 2. Step plot showing redshift distribution for isolated galaxies (iso) and non-isolated galaxies (nis) for the star-forming (blue top-left panel), composite (green top-right panel), Seyfert (red bottom-left panel) and LINER (orange bottom-right panel) galaxies.

where β and α are slope and intercept, respectively. Aiming at studying how the environment affects the SFR relative to the M_* for the SF, composite, Seyfert and LINER classified sub-samples of galaxies, we generate the equation of the best-fitted line of the SF galaxies (the equation of MS based on Eq. (5)). This best-fitted line is used as a reference to understand the behaviour of SFR relative to M_* for all other sub-samples of galaxies residing in different environments. Figs. 3, 4, 5 and 6 show the distributions of SFR with respect to M_* of the SF, composite, Seyfert and LINER galaxies for isolated and non-isolated cases along with the corresponding best-fitted MS line of the SF galaxies. The width of the MS of ± 0.3 dex (dashed lines) in these figures is adopted from Refs. [9, 14, 19, 42]. The figures show the positions of galaxies of all sub-samples with respect to the MS and the corresponding numbers of galaxies with their percentages are shown in Table I. Furthermore, the galaxies are divided into the redshift slices containing a binning size of 0.01 aiming to decrease the Malmquist bias as detailed in Ref. [43]. Table II shows the Kolmogorov-Smirnov (KS) test for all redshift slices, a test that uses statistical probability to assess the degree of similarity between the two independent distributions. The larger probability value ($P > 0.05$) indicates that there is no significant difference between the distributions, which implies that the two distributions are the same, while a small probability value ($P < 0.05$) indicates the existence of a significant difference between the distributions, which implies that the two distributions are different [44].

The general equations of the best-fitted line for the isolated and non-isolated galaxies for our data are respectively given by

$$\log_{10}(\text{SFR}) = 0.72 \log_{10}(M_*) - 7.06, \quad (6)$$

$$\log_{10}(\text{SFR}) = 0.70 \log_{10}(M_*) - 6.89. \quad (7)$$

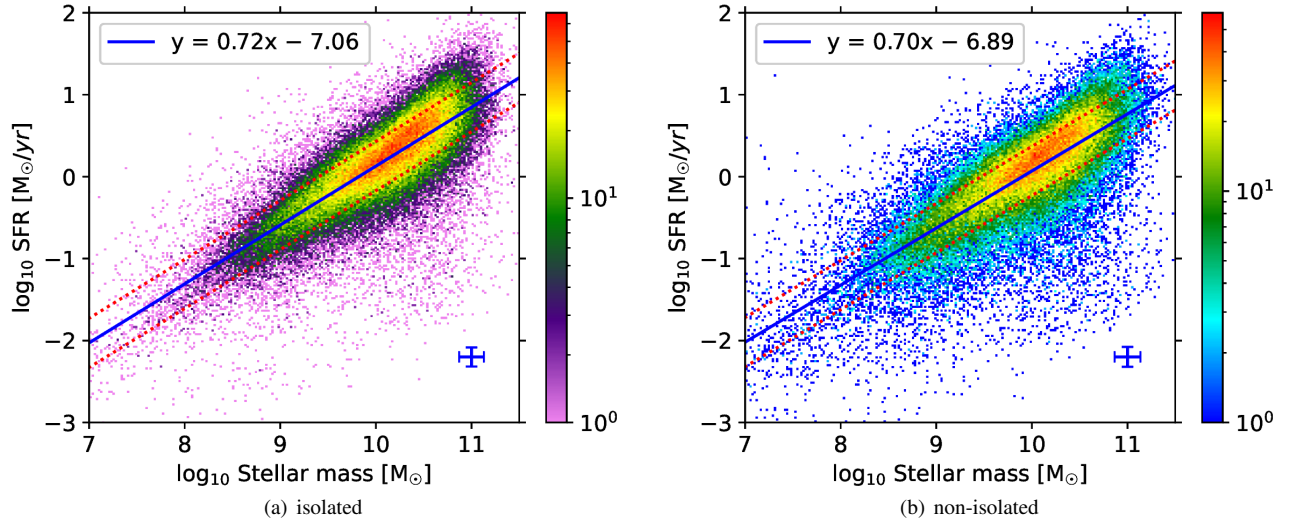


FIG. 3. Scatter plots showing SFR as the function of stellar mass for isolated (left plot) and non-isolated (right plot) star-forming galaxies. The violet, indigo, green, yellow and red colours in the left plot respectively show the 0%, 25%, 50%, 75% and 100% of the probability distributions for isolated star-forming galaxies, while the blue, cyan, green, yellow and red colours in right plot respectively show the 0%, 25%, 50%, 75% and 100% of the probability distributions for non-isolated star-forming galaxies. The right-bottom cross bars on each diagram correspond to 2σ Poissonian error in the calculated values of stellar mass and the SFR.

Table III indicates the percentage change between isolated and non-isolated galaxies above MS, within MS and below MS for SF (column 2), composite (column 3), Seyfert (column 4) and LINER (column 5) galaxies. This table is used as the tracer on how the positioning of galaxies in the plane of SFR versus M_* and hence the SFR are affected by changing the environment in which the galaxies reside.

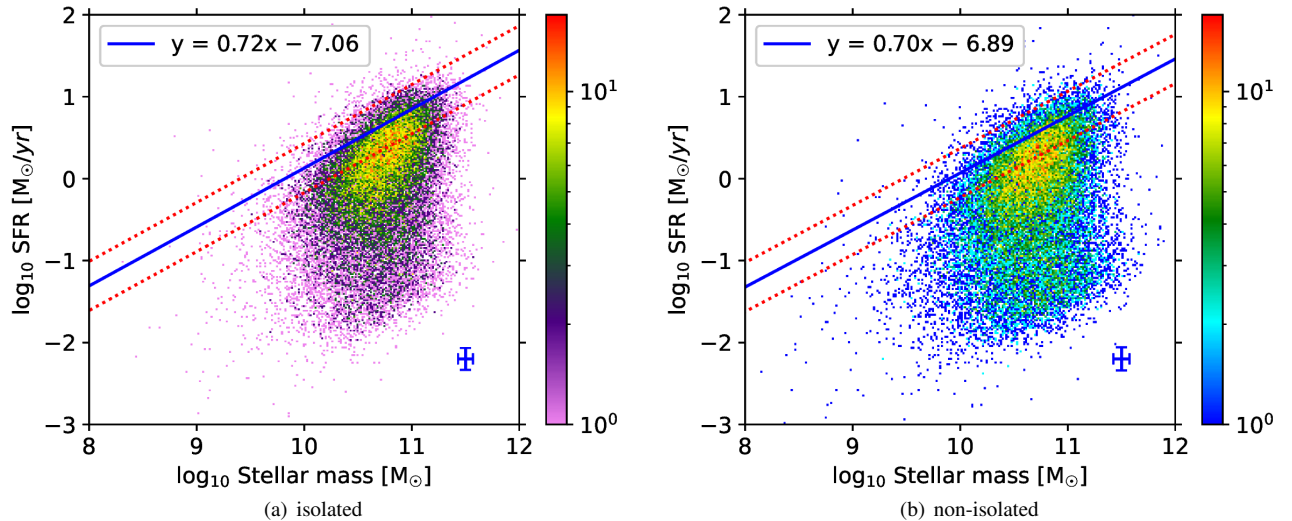


FIG. 4. Scatter plots showing SFR as the function of stellar mass for isolated (left plot) and non-isolated (right plot) composite galaxies. The violet, indigo, green, yellow and red colours in the left plot respectively show the 0%, 25%, 50%, 75% and 100% of the probability distributions for isolated composite galaxies, while the blue, cyan, green, yellow and red colours in the right plot show respectively the 0%, 25%, 50%, 75% and 100% of the probability distributions for non-isolated composite galaxies. The right bottom cross bars on each diagram correspond to 2σ Poissonian error in the calculated values of stellar mass and the SFR.

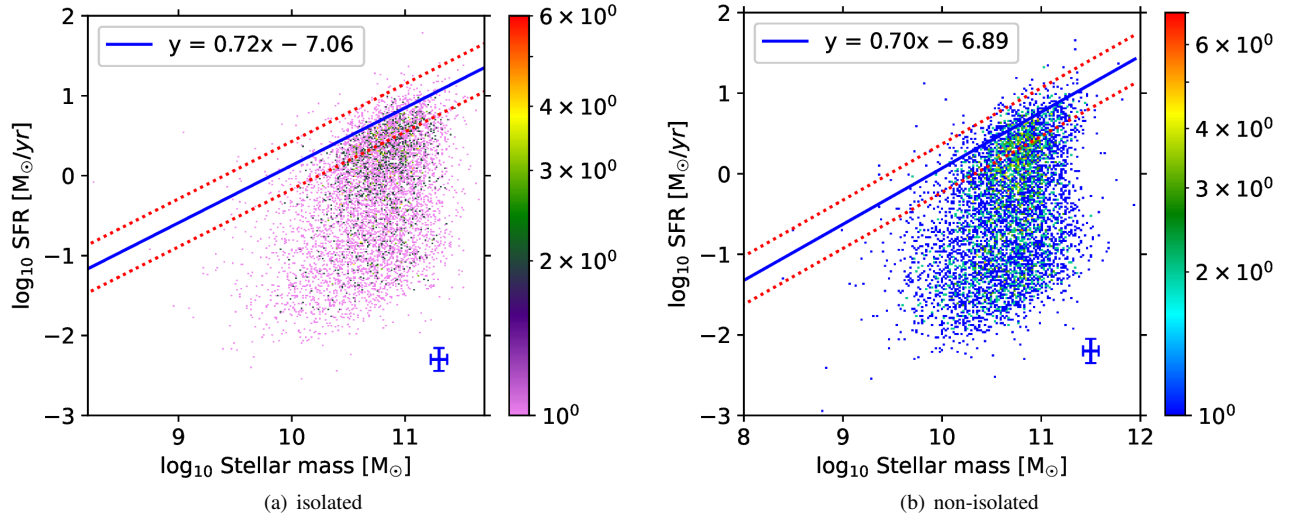


FIG. 5. Scatter plots showing SFR as the function of stellar mass for isolated (left plot) and non-isolated (right plot) Seyfert galaxies. The violet, indigo, green, yellow and red colours in the left plot respectively show the 0%, 25%, 50%, 75% and 100% of the probability distributions for isolated Seyfert galaxies, while the blue, cyan, green, yellow and red colours in the right plot show respectively the 0%, 25%, 50%, 75% and 100% of the probability distributions for non-isolated Seyfert galaxies. The right bottom cross bars on each diagram correspond to 2σ Poissonian error in the calculated values of stellar mass and the SFR.

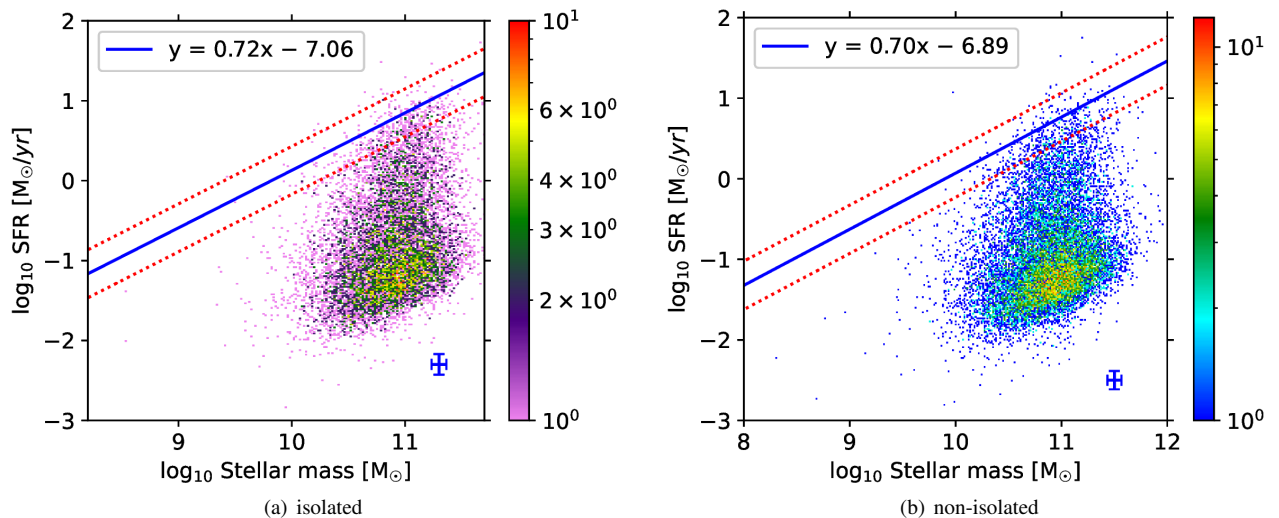


FIG. 6. Scatter plots showing SFR as the function of stellar mass for isolated (left plot) and non-isolated (right plot) LINERs. The violet, indigo, green, yellow and red colours in the left plot respectively show the 0%, 25%, 50%, 75% and 100% of the probability distributions for isolated LINERs, while the blue, cyan, green, yellow and red colours in the right plot show respectively the 0%, 25%, 50%, 75% and 100% of the probability distributions for non-isolated LINERs. The right bottom cross bars on each diagram correspond to 2σ Poissonian error in the calculated values of stellar mass and the SFR.

B. Quenching and Colour Bimodality

Galaxies can be categorized into two groups: those actively forming stars, appearing blue, and those lacking significant star formation, appearing red. The galaxies initially fall into blue sub-category and then they change gradually to red [45, 46]. It is clear to say that evolution from one category to another must involve processes which quench their rate of forming new stars from the blue cloud passing the intermediate stage (green valley) to the red sequence [47, 48]. The factors for this transformation may be due to internal mechanisms like negative feedback from the AGNs and the galaxy environment. To study the effect of the environment on quenching, Table IV shows the number of galaxies with respect to the green valley (GV) for isolated and non-isolated galaxies respectively, and the position of galaxies on the colour against the stellar mass diagrams are shown in Figs. 7(a), 7(b), 7(c) and 7(d) for the SF, composite, Seyfert and LINER galaxies respectively. The width of the GV is derived

TABLE I. The number of galaxies within (MS), above (Above MS), and below (Below MS) the star-forming main sequence for isolated (iso) and non-isolated (nis) environments.

Position (1)	Star-forming (%)		Composite (%)		Seyfert (%)		LINERs (%)	
	iso (2)	nis (3)	iso (4)	nis (5)	iso (6)	nis (7)	iso (8)	nis (9)
MS	65164(69.53)	50614(65.67)	8418(27.46)	6630(23.59)	1376(20.71)	1123(19.06)	433(3.81)	391(2.52)
Above MS	16720(17.84)	12915(16.76)	304(0.99)	275(0.98)	41(0.62)	36(0.61)	20(0.18)	14(0.09)
Below MS	11843(12.64)	12541(17.57)	21930(71.55)	21206(75.44)	5226(78.67)	4734(80.33)	10902(96.01)	15098(97.39)
Total	93727(100)	77070(100)	30652(100)	28111(100)	6643(100)	5893(100)	11355(100)	15503(100)

TABLE II. The Kolmogorov-Smirnov probability values for stellar mass $P(M_*)$ and star formation rate $P(\text{SFR})$ within the redshift bin size of 0.01.

Redshift (1)	$P(M_*)$				$P(\text{SFR})$			
	Star-forming (2)	Composite (3)	Seyfert (4)	LINERs (5)	Star-forming (6)	Composite (7)	Seyfert (8)	LINERs (9)
$z < 0.04$	2.3×10^{-22}	2.16×10^{-10}	0.0109	9.54×10^{-16}	3.91×10^{-7}	5.54×10^{-18}	0.324	9.416×10^{-6}
$0.04 \leq z < 0.05$	5.07×10^{-9}	5.16×10^{-7}	0.055	6.6×10^{-10}	3.34×10^{-8}	8.12×10^{-8}	0.774	0.8403
$0.05 \leq z < 0.06$	6.48×10^{-7}	0.000122	0.0139	4.71×10^{-10}	0.000485	1.83×10^{-10}	0.277	0.08203
$0.06 \leq z < 0.07$	2.84×10^{-11}	2.75×10^{-7}	0.629	1.82×10^{-15}	7.39×10^{-5}	6.26×10^{-9}	1.7×10^{-5}	0.0263
$0.07 \leq z < 0.08$	2.35×10^{-12}	1.23×10^{-13}	0.0158	6.66×10^{-10}	4.93×10^{-5}	5.22×10^{-8}	0.0192	0.1355
$0.08 \leq z < 0.09$	2.17×10^{-8}	4.48×10^{-9}	0.153	2.43×10^{-8}	0.00233	4.7×10^{-5}	0.401	0.1036
$0.09 \leq z < 0.10$	7.9×10^{-9}	2.67×10^{-16}	0.00465	3.64×10^{-9}	0.00988	0.000148	0.742	0.04011
$0.10 \leq z < 0.11$	0.00027	1.22×10^{-10}	0.518	6.36×10^{-9}	0.0067	0.0162	0.412	0.00207
$0.11 \leq z < 0.12$	0.000166	6.98×10^{-6}	0.000509	0.000901	0.0107	0.000455	0.0254	0.8636
$0.12 \leq z < 0.13$	8.13×10^{-5}	3.07×10^{-5}	0.173	1.55×10^{-9}	0.006	5.65×10^{-5}	0.00857	0.02497
$0.13 \leq z < 0.14$	0.000142	4.5×10^{-11}	0.12	7.32×10^{-8}	0.002	2.66×10^{-5}	0.599	0.01283
$0.14 \leq z < 0.15$	0.0492	0.000808	0.00162	0.00602	0.0047	0.0237	0.19	0.04616
$0.15 \leq z < 0.16$	0.0111	6.93×10^{-5}	0.129	0.0225	0.395	0.0508	0.216	0.02163
$0.16 \leq z < 0.17$	0.184	0.000254	0.731	0.0206	0.913	0.541	0.0246	0.003163
$z \geq 0.17$	0.2	0.000803	0.717	0.000157	0.177	0.0744	0.2	0.04614

TABLE III. The percentage change (Δ (%)) of isolated and non-isolated galaxies within MS, above MS and below MS.

Position (1)	Δ (%)			
	Star-forming (2)	Composite (3)	Seyfert (4)	LINERs (5)
MS	3.86	3.87	1.65	1.29
Above MS	1.08	0.01	0.01	0.09
below MS	4.93	3.89	1.66	1.38
Total	9.88 ~ 10	7.77 ~ 8	3.32 ~ 3	2.76 ~ 3

following the Ref. [49], which is obtained from equations,

$$u - r = -0.24 + 0.25 \times M_*, \quad (8)$$

$$u - r = -0.75 + 0.25 \times M_*. \quad (9)$$

Here u and r magnitudes were derived from the SDSS database with extinction corrected, stellar mass is in the unit of M_\odot . Table V indicates the percentage change between isolated and non-isolated galaxies above GV, within GV and below GV for the SF (column 2), composite (column 3), Seyfert (column 4) and LINERs (column 5). This table trace how the positioning of galaxies in the colour against stellar mass diagram and hence quenching are affected by changing the galaxies' environment.

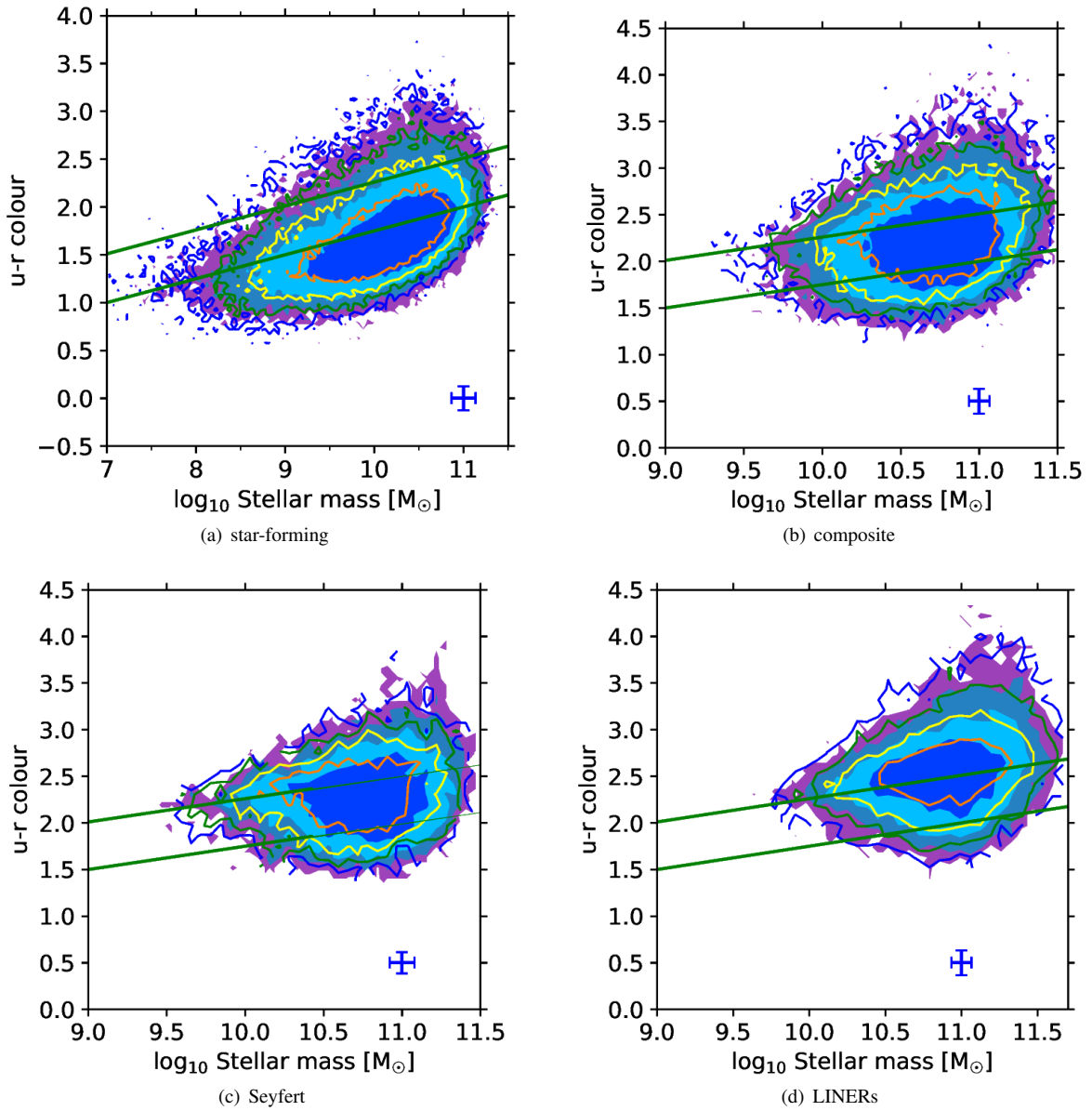


FIG. 7. Distribution of galaxy's rest-frame colour against stellar mass for star-forming (top-left plot), composite (top-right plot), Seyfert (bottom-left plot) and LINER (bottom-right plot) galaxies. The filled contour plots are for the isolated galaxies while the non-filled contour plots are for the non-isolated galaxies. Contours are drawn at 25%, 50%, 75% and 100% of the maximum density of each classified galaxy. The cross bars correspond to 2σ Poissonian error in the calculated values of stellar mass and rest-frame colour.

TABLE IV. The number of galaxies within the green valley (GV), above the green valley (Above GV), and below the green valley (Below GV) for isolated (iso) and non-isolated (nis) galaxies.

Position (1)	Star-forming (%)		Composite (%)		Seyfert (%)		LINERs (%)	
	iso (2)	nis (3)	iso (4)	nis (5)	iso (6)	nis (7)	iso (8)	nis (9)
GV	28401(30.30)	26810(34.79)	15754(51.40)	13643(48.53)	3284(49.44)	2857(48.48)	4234(37.29)	5198(33.53)
Above GV	5745(6.13)	6394(8.29)	8411(27.44)	10206(36.31)	2228(33.53)	2331(39.56)	6524(57.45)	9756(62.93)
Below GV	59581(63.57)	43866(56.92)	6487(21.16)	4262(15.16)	1131(17.03)	705(11.96)	597(5.26)	549(3.54)
Total	93727(100)	77070(100)	30652(100)	28111(100)	6643(100)	5893(100)	11355(100)	15503(100)

TABLE V. The percentage change (Δ (%)) of isolated and non-isolated galaxies within the green valley (GV), above the green valley (Above GV) and below the green valley (below GV).

Position (1)	Δ (%)			
	Star-forming (2)	Composite (3)	Seyfert (4)	LINERs (5)
GV	4.49	2.87	0.96	3.76
Above GV	2.26	8.87	2.03	4.48
below GV	8.85	6.00	5.07	0.76
Total	15.60 ~ 16	17.74 ~ 18	8.06 ~ 8	9.00 ~ 9

TABLE VI. The Kolmogorov-Smirnov probabilities for colour $P(u - r)$ within the redshift binning size of 0.01 involving star-forming, composite, Seyfert and LINER galaxies.

Redshift (1)	$P(u - r)$			
	Star-forming (2)	Composite (3)	Seyfert (4)	LINERs (5)
$z < 0.04$	2.25×10^{-51}	3.16×10^{-18}	0.00151	6.06×10^{-4}
$0.04 \leq z < 0.05$	3.42×10^{-16}	9.45×10^{-11}	0.661	0.536
$0.05 \leq z < 0.06$	3.68×10^{-17}	1.39×10^{-7}	0.179	4.65×10^{-5}
$0.06 \leq z < 0.07$	2.84×10^{-11}	9.42×10^{-13}	3.54×10^{-7}	0.611
$0.07 \leq z < 0.08$	2.52×10^{-20}	3.68×10^{-12}	0.0294	0.467
$0.08 \leq z < 0.09$	2.54×10^{-5}	4.47×10^{-11}	0.966	0.116
$0.09 \leq z < 0.10$	1.04×10^{-7}	5.9×10^{-11}	0.0487	0.314
$0.10 \leq z < 0.11$	0.00859	4.17×10^{-6}	0.224	0.475
$0.11 \leq z < 0.12$	0.00142	2.13×10^{-6}	0.053	0.0087
$0.12 \leq z < 0.13$	0.000105	6.25×10^{-6}	0.013	0.481
$0.13 \leq z < 0.14$	6.84×10^{-5}	3.77×10^{-6}	0.446	0.011
$0.14 \leq z < 0.15$	0.00135	0.000201	0.0421	0.0081
$0.15 \leq z < 0.16$	0.0297	0.00409	0.00346	0.0821
$0.16 \leq z < 0.17$	0.0788	0.00759	0.724	0.0161
$z \geq 0.17$	0.0547	0.019	0.878	0.0504

IV. DISCUSSION

From columns (2), (3) and (5) of Table II it is observed that the SF, composite and LINER stellar masses depend on the environment resulting from having probability values less than 0.05 that is ~ 0.02 , $\sim 2.95 \times 10^{-4}$, and ~ 0.02 on average, respectively. The relationships of their masses with the environment decrease with the increase in redshift. From columns (6) and (7) of Table II it is observed that the SF and composite SFR depend on the environment for low redshift ($z \lesssim 0.15$) although at higher redshift ($z > 0.15$) they are only mildly influenced by the environment. From column (9), we observe that there is a weak dependence of LINER SFR on the environment across all redshift ranges. This result is supported by the findings from simulations based on the density approach reported in Ref. [50]. From columns (4) and column (8) of this table it is observed that the Seyfert galaxies' stellar mass and SFR weakly depend on the environment, this results from having probability value of ~ 0.2 and ~ 0.3 on average for M_* and SFR respectively, which are much larger than 0.05 (the standard probability value in statistics). This implies that there is no significant difference in measurements of M_* and SFR between the two corresponding distributions.

In summary, composite galaxies have lower M_* and higher SFR than Seyfert which has lower M_* and higher SFR than LINERs. The stellar mass of SF, composite, and LINERs depends on the environment while the stellar mass of Seyfert weakly depends on the environment. The SFR of SF and composite galaxies depends on the environment at lower redshift (in this case $z \lesssim 0.15$), for higher redshift (in this case $z > 0.15$) the dependence of SFR on the environment for SF and composite galaxies is very weak. The SFR of Seyfert and LINERs weakly depend on the environment following the evidence from the KS probability values in Table II. These results support the findings in Refs. [19–24] indicating that the SF galaxies in dense regions of the universe have suppressed SFRs. However, these results disagree with findings by Ref. [25] using the density approach which observed a strong dependence of AGNs stellar mass and SFR on environment. On the other hand, the study agrees with Ref.

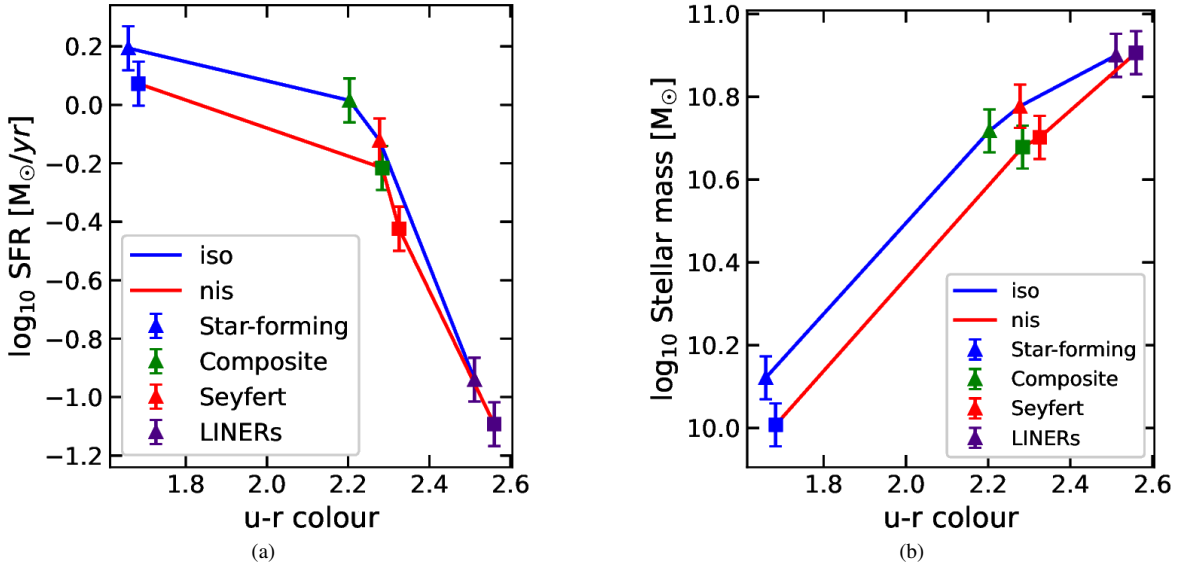


FIG. 8. Variation of median star formation rate versus the reddening-corrected rest-frame colour (left panel), and median stellar mass versus the reddening-corrected rest-frame colour (right panel) for star-forming (blue points), composite (green points), Seyfert (red points) and LINER (indigo points) galaxies. The error bar corresponds to 1σ Poissonian error in SFR and stellar mass. The solid lines are used to connect the median values of all these subclasses of galaxies residing in isolated and non-isolated environments respectively.

[25] on one side that the fraction of low-density AGNs is larger than the sample of higher-density AGNs. This study revealed that the fact is valid for isolated and non-isolated galaxies at lower redshift (in this case $z > 0.09$) as shown in Fig. 2, the fraction of non-isolated galaxies is higher than isolated galaxies. For the case of $z \lesssim 0.09$, the fraction of isolated Seyfert and LINERs (AGNs) is larger than the sample of non-isolated AGNs. This relation is not only valid for AGNs but also SF and composite galaxies. The study revealed that non-isolated galaxies reside mostly at the lower redshift while the isolated galaxies reside at higher redshift for all the classified galaxies.

The equations of the main sequence for SF galaxies in Fig. 3 show a tight relationship between the $\log(\text{SFR})$ and $\log(M_{\star})$ as explained in Section III. From Fig. 4, 5, 6 it is observed that the loci of SFR versus stellar mass for composite, Seyfert and LINER galaxies respectively, are almost perpendicular to the SF MS. Composite galaxies having extended interval in SFR, +1 dex above to -2 dex below the MS, Seyfert lie below the MS between the SFR range 0.5 to -2.5 dex, while LINERs lie more below the MS between the SFR range 0 to -2.5 dex. These results are consistent with the findings by Refs. [1, 14, 19, 51]. It is observed that isolated SF MS in Fig. 3(a) deviate from the non-isolated SF MS in Fig. 3(b) by 0.02 dex and 0.17 dex in slope and intercept, respectively. This indicates that the SFR decreases for non-isolated galaxies when compared to isolated galaxies. From Fig. 4 it is evident that composite galaxies possess stellar masses greater than $10^{10} M_{\odot}$, unlike the SF galaxies, the SFR of composite galaxies shows almost no relation with M_{\star} . The shapes of composite galaxies distribution stretch beyond the highest point of the SF MS, this area with high SFRs may indicate galaxies experiencing vigorous bursts of star formation, showing consistent results with Refs. [10, 52–54]. The composite galaxies span from the higher mass part of the main sequence to a minimal active star formation region. Composite galaxies have a greater average stellar mass compared to purely SF galaxies, yet their average SFR is lower means the onset of star-formation suppression may have begun during the composite stage, this is consistent with the results from Refs. [14, 55]. From Fig. 6 it is evident that most LINERs fall below the SF MS, this indicates that they have very little current star formation activities compared to Seyfert galaxies as shown by Fig. 5, which is consistent with the results from Refs. [14, 39] that LINERs are mostly observed in the older stellar population.

Observations from Table I indicate that the non-isolated environment increases the rate of quenching, this is indicated by the higher percentage of galaxies below the MS when compared with the isolated environment. Furthermore, the lower percentage of the number of galaxies within and above the MS for the non-isolated environment indicates the decrease of SFR for this environment compared to the isolated one. From Table III it is observed that the total percentage change of galaxies in isolated and non-isolated environments for SF galaxies is $\sim 10\%$, for composite is $\sim 8\%$, for Seyfert and LINERs is only $\sim 3\%$ indicating that the quenching of SF and composite galaxies depends on the environment while the quenching of the AGNs (Seyfert and LINERs) have very weak dependence on the environment. This result of the weak dependence of SFR for Seyfert and LINERs on the environment is also indicated in Table II showing higher KS probabilities on these galaxies.

The $u-r$ colour against M_{\star} diagrams in Figs. 7(a), 7(b), 7(c), and 7(d) reinforce the relation with respect to the MS in Figs. 3, 4, 5 and 6, respectively. The composite galaxies are more redder and massive than the SF, the Seyfert galaxies are more massive and redder than composite, and LINERs have the highest stellar mass and most redder, this observations are in line with the

finding by Ref. [14]. Table IV, indicates that the non-isolated environment increases the rate of quenching, this is indicated by the higher percentage of galaxies above the green valley (Above GV) and within the green valley (GV) when compared with the isolated environment. Furthermore the lower percentage of number of galaxies below the green valley for non-isolated galaxies when compared to isolated galaxies indicates the decrease of SFR for non-isolated galaxies. From Table V it is observed that the total percentage change of galaxies in isolated and non-isolated environments for SF galaxies is $\sim 16\%$, for composite is $\sim 18\%$, indicating that quenching of SF and composite galaxies depends on the environment supported by Fig. 7(a) and 7(b) whereby the contour plot for the non-isolated galaxies (non-filled contour) are seen to diverge from the isolated SF galaxies (filled contour). For Seyfert and LINERs, the percentage change is only $\sim 8\%$ and $\sim 9\%$ respectively, indicating that quenching of AGNs (Seyfert and LINERs) has a weak dependence on the environment. From Figs. 7(c) and 7(d) it is observed that the colour against stellar mass relationships for Seyfert and LINERs show deviation for isolated (filled contour) and non-isolated (non-filled contour), but the deviation is insignificant and less than SF and composite galaxies as observed in Table V, indicating weak dependence of Seyfert and LINERs on the environment. Again these results arise from the weak dependence of SFR for Seyfert and LINERs on the environment supporting the evidence derived from columns (8) and (9) of Table II and columns (4) and (5) of Table III. Furthermore, all these results are supported by the KS probability values for u-r colour in Table VI where columns (2) and (3) indicate that SF and composite galaxies' u-r colour depend on the environment by having average probability values of ~ 0.01 and $\sim 4.51 \times 10^{-3}$ respectively, which are smaller than the standard probability value in statistics (0.05), while columns (4) and (5) indicate that u-r colour of Seyfert and LINERs weakly depend on the environment by having average probability values of ~ 0.3 and ~ 0.2 respectively, which are much larger than the standard probability value. Again from Table VI it is seen that the relationship of u-r colour with the environment decreases with the increase in redshift.

It is observed that the SF galaxies in Fig. 7(a) form a blue cloud since most of the galaxies are below the green valley ($\sim 60\%$) as shown in Table IV while the composite galaxies in Fig. 7(b) form a green valley as most of the galaxies lie within demarcation lines ($\sim 50\%$) on average. Moreover, the evidence from Table IV indicates that most of Seyfert galaxies are within the green valley ($\sim 49\%$) on average and LINERs are above the green valley ($\sim 60\%$) on average, these support the observations from Figs. 7(c) and 7(d). Therefore from Table IV and Figs. 7 it is clear to say that composite, Seyfert and LINERs populate the green valley and red-sequence while SF galaxies populate the blue cloud, which also was observed by Refs. [15, 16, 56–58].

The observation from the right panel of Fig. 8 indicates that the average stellar mass increases in the sequence of SF, composite, Seyfert and LINERs while the left panel of Fig. 8 indicates that the average SFR decreases in the same sequence, agreeing with the findings by Ref. [59] which observed that galaxies hosting AGNs (in this case Seyfert and LINERs) are preferentially more massive and have low SFR. Fig. 8(a) also indicates that quenching of SFR increases from SF to composite, Seyfert and LINERs galaxies in which the dependence on the environment is seen to decrease at $SFR \sim -0.2$, which is equivalent to $M_\star = 10^{10.7} M_\odot$ as shown by Fig. 8(b). This implies that other mechanisms, for example, the AGNs feedback are responsible for quenching of galaxies with $M_\star \geq 10^{10.7} M_\odot$.

V. SUMMARY AND CONCLUSION

For the first time, we use the catalogue of groups and clusters derived by Ref. [32] from Sloan Digital Sky Survey as detailed in Refs. [30, 31], and the MPA-JHU data obtained using the methods outlined in Ref. [35, 36], to include the composite, Seyfert and LINERs on the local star formation MS then to study the influence of isolated and non-isolated environments on the star formation MS, colour bimodality and hence quenching of SFR. We apply the signal-to-noise criteria 3, to obtain a total of 274 517 galaxies. Again by removing the galaxies with no stellar mass and SFR measurements a total of 268 954 galaxies was obtained. The galaxies are classified based on emission line ratio using the NII diagnostic diagram obtaining 170 797 (63%) SF, 58 763 (22%) composite, 12 536 (5%) Seyfert and 26 858 (10%) LINERs. Using the catalog of groups and clusters by Ref. [32] we divide galaxies with no neighbour ($N_{gal} = 1$) as isolated, while the galaxies with more than one neighbour ($N_{gal} \geq 2$) as non-isolated. The final dataset contains 93 727 (55%), 77 070 (45%) SF galaxies, 30 652 (52%), 28 111 (48%) composite galaxies, 6 643 (53%), 5 893 (47%) Seyfert galaxies, and 11 355 (42%), 15 503 (58%) LINER galaxies with isolated and non-isolated environments respectively. Our results suggest that:

1. Non-isolated galaxies preferentially reside at lower redshift regions (in this case $z \lesssim 0.09$) while the isolated galaxies reside at higher redshift regions (in this case $z > 0.09$) of the universe.
2. SFR and stellar mass of SF and composite galaxies depend on the environment where high-mass galaxies are found in the isolated environment while the low-mass galaxies is a characteristic of the non-isolated environment. Furthermore, the isolated environment contains galaxies with high SFR while the non-isolated environment contains galaxies with low SFR. The dependence of M_\star and SFR on the environment decreases as the redshift increases.
3. Stellar masses of LINERs depend on the environment like SF and composite galaxies but its SFR weakly depends on the environment. Whereas the dependence of stellar mass and SFR of Seyfert galaxies on the environment is very weak. This implies that emission from AGNs (in this case Seyfert and LINERs) weakens the dependence of SFR on the environment.

4. The decrease of the slope for the MS of SF galaxies by 0.02 dex and intercept by 0.17 dex are observed between isolated and non-isolated galaxies implying that the environment is among the factors shaping the star formation main sequence.
5. There is a significant difference in the measurement of u-r colour for the SF and composite galaxies between the isolated and non-isolated environments while this difference for Seyfert and LINERs is insignificant. This implies that there is a weak dependence of u-r colour on the environment for Seyfert and LINERs.
6. SF, composite, Seyfert and LINER galaxies form evolutionary pathways where most SF galaxies are found in the blue cloud ($\sim 60\%$), both composite ($\sim 50\%$) and Seyfert ($\sim 49\%$) in the green valley, and LINERs ($\sim 60\%$) in the red sequence.
7. The dependence of quenching on the environment decreases at $M_{\star} = 10^{10.7} M_{\odot}$ indicating that for $M_{\star} \geq 10^{10.7} M_{\odot}$ other mechanisms (including the AGNs feedback) dominate the quenching process.

In the future, as the follow-up of this work, we will classify galaxies based on morphology, aiming to investigate what factor takes the reading on the dependance of galaxy properties on environment by comparing the isolated, group and cluster galaxies.

ACKNOWLEDGEMENTS

PP acknowledges support from The Government of Tanzania through the India Embassy, Mbeya University of Science and Technology (MUST) for Funding and SDSS for providing data. UDG is thankful to the Inter-University Centre for Astronomy and Astrophysics (IUCAA), Pune, India for the Visiting Associateship of the institute.

-
- [1] J. Speagle, C. Steinhardt, P. Capak, J. Silverman et al. *A Highly Consistent Framework for the Evolution of the Star-Forming” Main Sequence” from $z \sim 0 - 6$* , *ApJS* **214**, 15 (2014) [arXiv:1405.2041].
 - [2] P. Behroozi, R. Wechsler, C. Conroy, *The average star formation histories of galaxies in dark matter halos from $z \sim 0 - 8$* , *ApJ* **770**, 57 (2013) [arXiv:1207.6105].
 - [3] K. Noeske, B. Weiner, S. Faber, C. Papovich et al. *Star formation in aegis field galaxies since $z= 1.1$: The dominance of gradually declining star formation, and the main sequence of star-forming galaxies*, *ApJ* **660**, L43 (2007) [arXiv:astro-ph/0701924].
 - [4] G. Rodighiero, E. Daddi, I. Baronchelli, A. Cimatti et al. *The lesser role of starbursts in star formation at $z = 2$* , *ApJL* **739**, L40 (2011) [arXiv:astro-ph/0701924].
 - [5] N. Reddy, M. Pettini, C. Steidel, A. Shapley et al. *The characteristic star formation histories of galaxies at redshifts $z \sim 2 - 7$* , *ApJ* **754**, 25 (2012) [arXiv:1205.0555].
 - [6] B. Salmon, C. Papovich, S. Finkelstein, V. Tilviy et al. *The relation between Star Formation Rate and Stellar Mass for Galaxies at $3.5 \leq z \leq 6.5$ in CANDELS*, *ApJ* **799**, 183 (2015) .
 - [7] P. Santini, A. Fontana, M. Castellano, M. Criscienco et al. *The star formation main sequence in the Hubble Space Telescope Frontier Fields*, *ApJ* **847**, 76 (2017) [arXiv:1706.07059].
 - [8] G. Magdis, E. Daddi, M. Béthermin, M. Sargent et al. *The evolving interstellar medium of star-forming galaxies since $z = 2$ as probed by their infrared spectral energy distributions*, *ApJ* **760**, 6 (2012) [arXiv:1210.1035].
 - [9] K. Whitaker, P. Dokkum, G. Brammer, M. Franx *The star formation mass sequence out to $z= 2.5$* , *ApJL* **754**, L29 (2015) [arXiv:1205.0547].
 - [10] Y. Peng, S. Lilly, K. Kovač, M. Bolzonella et al. *Mass and Environment as Drivers of Galaxy Evolution in SDSS and zCOSMOS and the Origin of the Schechter Function*, *ApJ* **721**, 193 (2010) [arXiv:1003.4747].
 - [11] N. Drory, M. Alvarez *The contribution of star formation and merging to stellar mass buildup in galaxies*, *ApJ* **680**, 41 (2008)[arXiv:0803.1489].
 - [12] K. Whitaker, M. Franx, J. Leja, P. Dokkum et al. *Constraining the Low-mass Slope of the Star Formation Sequence at $0.5 < z < 2.5$* , *ApJ* **795**, 104 (2008)[arXiv:1407.1843].
 - [13] A. Renzini, Y. Peng, *An objective definition for the main sequence of star-forming galaxies*, *ApJ* **801**, L29 (2008)[arXiv:1502.01027].
 - [14] S. Leslie, L. Kewley, D. Sanders, N. Lee *Quenching star formation: insights from the local main sequence*, *MNRAS* **455**, L82 (2015) [arXiv:1509.03632].
 - [15] K. Schawinski, D. Thomas, M. Sarzi, C. Maraston et al. *Observational evidence for AGN feedback in early-type galaxies*, *MNRAS* **382**, 1415 (2007) [arXiv:0709.3015].
 - [16] K. Nandra, A. Georgakakis, C. Willmer, M. Cooper et al. *AEGIS: The color-magnitude relation for X-ray-selected active galactic nuclei*, *ApJ* **660**, L11 (2007).
 - [17] D. Croton, V. Springel, S. White, G. Lucia et al. *The many lives of active galactic nuclei: cooling flows, black holes and the luminosities and colours of galaxies*, *MNRAS* **365**, 11 (2013) [arXiv:astro-ph/0508046].
 - [18] D. Rosario, P. Santini, D. Lutz, L. Shao et al. *The mean star formation rate of X-ray selected active galaxies and its evolution from $z \sim 2.5$: results from PEP-Herschel*, *A & A* **545**, A45 (2012) [arXiv:1203.6069].

- [19] D. Elbaz, E. Daddi, D. Borgne, M. Dickinson et al. *The reversal of the star formation-density relation in the distant universe*, *A&A* **468**, 33 (2007) [arXiv:astro-ph/0703653].
- [20] I. Lewis, M. Balogh, R. Propris, W. Couch, R. Bower et al. *The 2dF Galaxy Redshift Survey: the environmental dependence of galaxy star formation rates near clusters*, *MNRAS* **334**, 673 (2002) [arXiv:astro-ph/0203336].
- [21] P. Gomez, R. Nichol, *Galaxy Star-Formation as a Function of Environment in the Early Data Release of the Sloan Digital Sky Survey*, *A&A* **584**, 210 (2003) [arXiv:astro-ph/0210193].
- [22] M. Tanaka, T. Goto, *The Environmental Dependence of Galaxy Properties in the Local Universe: Dependence on Luminosity, Local Density, and System Richness*, *AJ* **128**, 2677 (2004) [arXiv:astro-ph/0411132].
- [23] M. Cooper, J. Newman, *The DEEP2 Galaxy Redshift Survey: The Role of Galaxy Environment in the Cosmic Star-Formation History*, *MNRAS* **383**, 1058 (2008) [arXiv:0706.4089].
- [24] S. Patel, B. Holden, *The Dependence of Star Formation Rates on Stellar Mass and Environment at $z \sim 0.8$* , *ApJ* **705**, L67 (2007) [arXiv:0910.0837].
- [25] X. Deng, P. Wu, X. Qian, C. Luo, *Environmental Dependence of Stellar Mass, Star Formation Rate, Specific Star Formation Rate, and AGN Activity for an Apparent Magnitude Limited Main Galaxy Sample of the SDSS DR7*, *PASJ* **64**, 93 (2012).
- [26] M. Martig, F. Bournaud, R. Teyssier, A. Dekel et al. *Morphological quenching of star formation: making early-type galaxies red*, *ApJ* **707**, 250 (2009) [arXiv:0905.4669].
- [27] G. Erfanianfar, P. Popesso, A. Finoguenov, D. Wilman et al. *Non-linearity and environmental dependence of the star-forming galaxies main sequence*, *MNRAS* **455**, 2839 (2016) [arXiv:1511.01899].
- [28] P. Lang, S. Wuyts, R. Somerville, N. Schreiber, R. Genzel et al. *Bulge Growth and Quenching since $z = 2.5$ in CANDELS/3D-HST*, *ApJ* **788**, 788 (2014) [arXiv:1402.0866].
- [29] P. Ade, N. Aghanim, *Planck 2015 results. XXIII. The thermal Sunyaev-Zeldovich effect–cosmic infrared background correlation*, *A&A* **594**, A23 (2016) [arXiv:1509.06555].
- [30] D. Eisenstein, D. Weinberg, *SDSS-III: Massive spectroscopic surveys of the distant universe, the Milky Way, and extra-solar planetary systems*, *AJ* **142**, 72 (2011) [arXiv:1101.1529].
- [31] S. Alam, F. Albareti, C. Prieto, *The Eleventh and Twelfth Data Releases of the Sloan Digital Sky Survey: Final Data from SDSS-III*, *ApJ* **219**, 12 (2015) [arXiv:1501.00963].
- [32] E. Tempel, T. Tuvikene, *Merging groups and clusters of galaxies from the SDSS data. The catalogue of groups and potentially merging systems*, *A&A* **602**, A100 (2017) [arXiv:1704.04477].
- [33] E. Tempel, A. Tamm, M. Gramann, *Flux- and volume-limited groups/clusters for the SDSS galaxies: catalogues and mass estimation*, *A&A* **566**, A1 (2014) [arXiv:1402.1350].
- [34] G. Kauffmann, S. White, *The Environmental Dependence of the Relations between Stellar Mass, Structure, Star Formation and Nuclear Activity in Galaxies*, *MNRAS* **353**, 713 (2004) [arXiv:astro-ph/0402030].
- [35] J. Brinchmann, S. Charlot, *The physical properties of star forming galaxies in the low redshift universe*, *MNRAS* **351**, 1151 (2004) [arXiv:astro-ph/0311060].
- [36] C. Tremonti, T. Heckman, *The Origin of the Mass–Metallicity Relation: Insights from 53,000 Star-Forming Galaxies in the SDSS*, *ApJ* **613**, 898 (2004) [arXiv:astro-ph/0405537].
- [37] C. Kennicutt, *Star Formation in Galaxies Along the Hubble Sequence*, *A&A* **39**, 189 (1998) [arXiv:astro-ph/9807187].
- [38] S. Salim, J. Lee, R. Davé, *On the Mass–Metallicity–Star Formation Rate Relation for Galaxies at $z \sim 2$* , *ApJ* **808**, 14pp (2015) [arXiv:1506.03080].
- [39] L. Kewley, B. Groves, G. Kauffmann, T. Heckman et al. *The host galaxies and classification of active galactic nuclei*, *MNRAS* **372**, 961 (2006) [arXiv:astro-ph/0605681].
- [40] G. Kauffmann, T. Heckman, C. Tremonti, J. Brinchmann et al. *The host galaxies of active galactic nuclei*, *MNRAS* **346**, 1055 (2003) [arXiv:astro-ph/0304239].
- [41] L. Kewley, M. Dopita, R. Sutherland, C. Heisler et al. *Theoretical modeling of starburst galaxies*, *ApJ* **556**, 121 (2001) [arXiv:astro-ph/0106324].
- [42] T. Shimizu, R. Mushotzky, M. Meléndez, M. Koss et al. *Decreased specific star formation rates in AGN host galaxies*, *MNRAS* **452**, 1841 (2007) [arXiv:1506.07039].
- [43] P. Teerikorpp, *Eddington-Malmquist bias in a cosmological context*, *A&A* **576**, A75 (2015) [arXiv:1503.02812].
- [44] D. Harari, S. Mollerach, *Kolmogorov-Smirnov test as a tool to study the distribution of ultra-high energy cosmic ray sources*, *A&A* **394**, 916 (2009) [arXiv:0811.0008].
- [45] T. Gonçalves, D. Martin, K. Menéndez-Delmestre, T. Wyder et al. *Quenching star formation at intermediate redshifts: downsizing of the mass flux density in the green valley*, *ApJ* **759**, 67 (2012) [arXiv:1209.4084].
- [46] J. Moustakas, A. Coil, J. Aird, M. Blanton, R. Cool et al. *Quenching star formation at intermediate redshifts: downsizing of the mass flux density in the green valley*, *ApJ* **767**, 50 (2013) [arXiv:1301.1688].
- [47] S. Faber, C. Willmer, C. Wolf, D. Koo, B. Weiner, J. Newman et al. *Galaxy Luminosity Functions to $z \sim 1$: DEEP2 vs. COMBO-17 and Implications for Red Galaxy Formation*, *ApJ* **665**, 265 (2007) [arXiv:astro-ph/0506044].
- [48] R. Hickox, J. Mullaney, D. Alexander, C. Chen, F. Civanoet al. *Black hole variability and the star formation–active galactic nucleus connection: do all star-forming galaxies host an active galactic nucleus*, *ApJ* **782**, 9 (2014) [arXiv:1306.3218].
- [49] K. Schawinski, C. Urry, B. Simmons, L. Fortson, S. Kaviraj et al. *The green valley is a red herring: Galaxy Zoo reveals two evolutionary pathways towards quenching of star formation in early- and late-type galaxies*, *MNRAS* **440**, 889 (2014).
- [50] G. Rihtaršič, V. Biffi, D. Fabjan, K. Dolag et al. *Environmental dependence of AGN activity and star formation in galaxy clusters from Magneticum simulations*, *A&A* **683**, A57 (2024) [arXiv:2307.06374].
- [51] E. Daddi, M. Dickinson, G. Morrison, R. Chary et al. *Multiwavelength study of massive galaxies at $z \sim 2$. I. Star formation and galaxy growth*, *ApJ* **670**, 156 (2007). [arXiv:0705.2831].

- [52] J. Rich, L. Kewley, M. Dopita, *Galaxy-Wide Shocks in Late-Merger Stage Luminous Infrared Galaxies*, *ApJ* **782**, 9 (2014) [[arXiv:1104.1177](#)].
- [53] S. Leslie, J. Rich, L. Kewley, M. Dopita, *The energy source and dynamics of infrared luminous galaxy ESO 148-IG002*, *MNRAS* **444**, 1842 (2014) [[arXiv:1408.0789](#)].
- [54] T. Yuan, L. Kewley, D. Sanders, *The Role of Starburst-Active Galactic Nucleus Composites in Luminous Infrared Galaxy Mergers: Insights from the New Optical Classification Scheme*, *ApJ* **709**, 884 (2010)
- [55] D. Schiminovich, T. Wyder, D. Martin, B. Johnson et al. *The UV-Optical Color Magnitude Diagram II: Physical Properties and Morphological Evolution On and Off of a Star-Forming Sequence*, *ApJS* **173**, 315 (2007) [[arXiv:0711.4823](#)].
- [56] V. Smolčić, G. Zamorani, E. Schinnerer, S. Bardelli et al. *Cosmic evolution of radio selected active galactic nuclei in the cosmos field*, *ApJ* **696**, 24 (2009) [[arXiv:0901.3372](#)].
- [57] K. Alatalo, K. Nyland, G. Graves, S. Deustua et al. *NGC 1266 as a local candidate for rapid cessation of star formation*, *ApJ* **780**, 186 (2014) [[arXiv:1311.6469](#)].
- [58] K. Alatalo, S. Cales, P. Appleton, L. Kewley et al. *Catching Quenching Galaxies: The Nature of the WISE Infrared Transition Zone*, *ApJL* **794**, L13 (2014) [[arXiv:1409.2489](#)].
- [59] X. Deng, Y. Xin, P. Wu, P. Jiang et al. *Some Properties of Active Galactic Nuclei in the Volume-limited Main Galaxy Samples of SDSS DR8*, *ApJ* **754**, 82 (2012).